Journal of Photochemistry and Photobiology A: Chemistry 217 (2011) 191–200

Contents lists available at ScienceDirect

Journal of Photochemistry and Photobiology A: Chemistry

journal homepage: www.elsevier.com/locate/jphotochem

Characteristics of microwaves on second generation nitrogen-doped TiO_2 nanoparticles and their effect on photoassisted processes

Satoshi Horikoshi[a,*], Yuya Minatodani[b], Hideki Sakai[a,b], Masahiko Abe[a,b], Nick Serpone[c,**]

[a] Research Institute for Science and Technology, Tokyo University of Science, 2641 Yamazaki, Noda, Chiba 278-8510, Japan
[b] Department of Pure and Applied Chemistry, Faculty of Science, Tokyo University of Science, 2641 Yamazaki, Noda, Chiba 278-8510, Japan
[c] Gruppo Fotochimico, Dipartimento di Chimica Organica, Universita di Pavia, Via Taramelli 10, Pavia 27100, Italy

ARTICLE INFO

Article history:
Received 20 July 2010
Received in revised form
28 September 2010
Accepted 9 October 2010
Available online 15 October 2010

Keywords:
N-doped TiO_2
In situ Raman spectroscopy
Photoactivity
4-Chlorophenol
Dielectric parameters
Second generation TiO_2 nanoparticles

ABSTRACT

Characteristics of 2.45-GHz microwave radiation were examined on two second generation nitrogen-doped TiO_2 nanomaterials prepared by annealing Degussa P-25 TiO_2 and Ishihara ST-01 TiO_2 at 400 °C and 500 °C, respectively, in air in the presence of urea, and for comparison on the undoped pristine samples. Band gaps of all four samples were determined by diffuse reflectance spectroscopy. Both the sizes and the BET specific surface areas of the TiO_2 particles were determined, together with dielectric constants and dielectric loss factors. Nitrogen doping caused the size to increase and surface area to decrease. Temperature–time profiles showed that the heating efficiency of the N-doped specimens by the microwaves was greater, particularly significant for the N-doped P25 sample, but rather small for the N-ST01 sample. The effect of microwaves on the surface optical phonons of the samples, with and without UV–vis irradiation, was examined by an *in situ* Raman spectroscopic technique; for the undoped P-25 and nitrogen-doped N-P25 TiO_2 systems the effect was negligible. By contrast, microwave irradiation of Ishihara ST-01 and nitrogen-doped N-ST01 TiO_2 samples showed significant changes in the 144-cm^{-1} optical phonons. Results infer a microwave thermal effect on the Ishihara ST-01 and N-ST01 specimens, whereas for the Degussa P-25 samples the microwaves also imparted a specific effect as the microwaves influenced the N-dopant sites in contrast to the ST-01 systems where the dopant sites were unaffected as evidenced by temperature–time profiles. The microwave-/photo-assisted degradation of 4-chlorophenol under various conditions of UV–vis irradiation and conventional heating, as opposed to microwave heating, confirms the specific microwave effect for the P-25 systems.

1. Introduction

The last few years have witnessed a growing interest in the use of microwave radiation as an attractive heating source in organic synthesis. Microwave-assisted organic syntheses have demonstrated increased product yields and increased shorter syntheses times (faster kinetics) than were otherwise seen by conventional heating [1]. High product yields and minimization, if not suppression, of side-products generation are some of the attractive features of microwave dielectric heating.

Photoassisted degradation processes in TiO_2 dispersions can be enhanced by the added assistance of microwave radiation in the remediation of wastewaters contaminated with such pollutants as dyes, polymers, surfactants, herbicides, and endocrine disruptors even under inferior photodecomposition conditions: (i) small quantities of TiO_2 used, (ii) low concentration of dissolved oxygen, and (iii) low light irradiance [2,3]. Microwave radiation optimizes the interactions between the TiO_2 surface (surface charge, and surface affinity) and the organic pollutants [4]. The influence of microwaves in the photodegradation of organic pollutants has been reported in several studies that used different batches of TiO_2 nanomaterials: for example, TiO_2 supported on active carbon [5]; F- and Si-modified TiO_2 [6]; TiO_2 grains [7]; and TiO_2 pellets [8].

The notion of irradiating TiO_2 specimens with microwaves would seem curious because the photon energy of the 2.45-GHz microwaves (1×10^{-5} eV) is several orders of magnitude lower than the band-gap energy (3.2 eV) of the TiO_2 semiconductor needed to activate these nanomaterials. An integrated microwave/photo-assisted methodology in wastewater treatment might have some advantages. In this technique, a feature of the reaction on the TiO_2 surface involves thermal and specific effects (e.g. non-thermal effect) originating from the absorption of microwave radiation by the metal-oxide particulates. A microwave specific effect has been inferred for P-25 TiO_2 and to be independent of crystal shape, particle size, and surface area [9]. Similar results were displayed by the Raney-Ni and Urushibara-Ni catalysts [10]. Differences between

* Corresponding author. Tel.: +81 471212439.
** Corresponding author.
E-mail addresses: horikosi@rs.noda.tus.ac.jp, horikosi007@hotmail.co.jp (S. Horikoshi), nick.serpone@unipv.it, nickser@alcor.concordia.ca (N. Serpone).

1010-6030/$ – see front matter © 2010 Elsevier B.V. All rights reserved.
doi:10.1016/j.jphotochem.2010.10.008

various TiO_2 batches with regard to microwave specific effect(s) were examined using microwaves with different frequencies [11], and by examining the effects of the microwaves' magnetic and electric fields [12] in photoassisted processes involving TiO_2 and ZnO nanomaterials. Increased formation of •OH radicals for various TiO_2 specimens exposed to microwave irradiation correlated with increased photoactivity [9]. The microwave specific effect, not encountered by conventional heating, infers that the composition and the electronic characteristics of the TiO_2 materials may be important factors.

The syntheses and characteristic features of second-generation visible-light-active TiO_2 photocatalysts have been described in two recent critical reviews by Serpone and coworkers [13,14]. In the present study, we examined two nitrogen-doped TiO_2 materials together with the undoped specimens to probe what effects the microwave radiation might impart on these second generation photocatalysts.

2. Experimental

2.1. Preparation and characterization of nitrogen-doped TiO_2 systems

2.1.1. Nitrogen doping of Degussa P-25 TiO_2

The process by which Degussa P-25 TiO_2 was nitrogen-doped to yield a titanium oxynitride (i.e. $TiO_{2-x}N_x$) was analogous to that reported by Rengifo-Herrera et al. [15] and by others [16,17]. The synthesis of nitrogen-doped TiO_2 powders (N–TiO_2) was optimized and ascertained using various conditions from exploratory experiments. For instance, urea (source of nitrogen) and Degussa P-25 TiO_2 (ratio, 1:2) were blended manually in a mortar for ca. 30 min, followed by annealing in air for about 1 h at 400 °C at a heating rate of 10 °C min^{-1}. Subsequently, the materials were washed three times with Milli-Q water and then dried at 100 °C. The nitrogen-doped P-25 TiO_2 powder is henceforth denoted N-P25.

2.1.2. Nitrogen doping of Ishihara ST-01 TiO_2

Powdered samples of nitrogen-doped TiO_2 were also prepared by mixing 1 g of the Ishihara ST-01 TiO_2 powder (Ishihara Sangyo Kaisha Ltd.) and 2 g of reagent grade urea in a crucible, after which the mixture was heated in an electric furnace at 500 °C for 3 h (heating rate, 5 °C min^{-1}). The preparation of this N-doped TiO_2 material was similar to the procedure used in the synthesis of sulfur-doped TiO_2 with thiourea [18]. Optimal conditions of temperature and mixture ratio were determined in prior exploratory experiments.

The band-gap energies of the pale yellow colored N-doped TiO_2 samples and of undoped TiO_2 powders were measured by diffuse reflectance UV/vis spectroscopy (DRS) using a JASCO V670 UV/vis/NIR spectrophotometer equipped with an ISN-723 integrating sphere unit. The Kubelka–Munk relation was used to transform the reflectance data into absorption spectra.

The Brunauer–Emmett–Teller (BET) surface areas of TiO_2 powdered samples were measured with a Yuasa-Ionics Ltd., Monosorb BET surface area analyzer. Particle sizes were determined by both transmission electron microscopy (TEM) using a Hitachi High-Technologies Co. H-7650 electron microscope (average size of 30 particles randomly selected), and by X-ray diffraction (XRD) using the Scherer equation [19] and the PANalytical X'Pert pro XRD system; the percent anatase content in the samples was also assessed with the latter system.

2.2. Experimental setup of microwave apparatus

Continuous microwave radiation was obtained using a Hitachi Kyowa Engineering Co. Ltd. 2.45-GHz microwave generator (maximal power, 800 W; Fig. 1) equipped with a power controller, a power monitor, and an isolator (air cooling device). The 60-W continuous microwaves emitted from the magnetron were measured using the power monitor. The reactor was sealed with two Byton O-rings and a stainless steel cap. A pressure gauge and a release bulb were connected to the cover of the reactor. The reaction mixture was magnetically stirred continuously. Unless noted otherwise, temperatures of the TiO_2 dispersions containing 4-chlorphenol and subjected to microwave irradiation were measured with a K-type thermocouple; temperatures reached a maximum of 114 °C after 13 min (inset of Fig. 1).

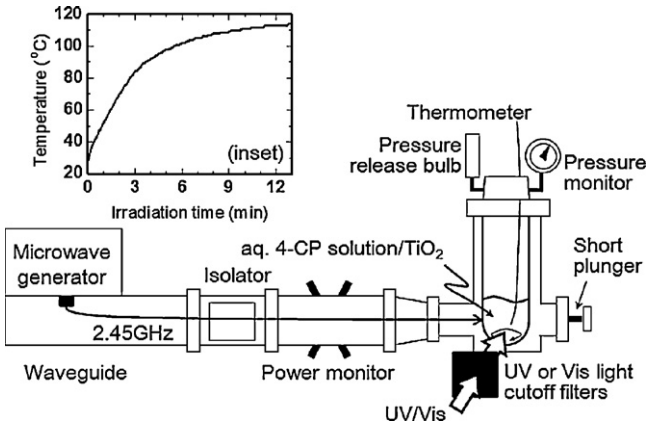

Fig. 1. Experimental setup used in the photoassisted decomposition of 4-CP in aqueous undoped and N-doped TiO_2 dispersions using an integrated UV/vis source and a source of MW radiation. UV wavelengths and visible radiation were obtained using various light cutoff filters. The inset in the figure shows the temperature profile of an aqueous 4-CP solution subjected to the TiO_2/UV–vis/MW method; the concentrations of 4-CP and undoped P-25 TiO_2 were 0.10 mM and 5 mg, respectively.

The two radiation sources (MW and UV/vis) were placed so that their radiation would cross at 90° at the center of the solution. The UV light transmitting filter ($\lambda < 400$ nm) and the UV cutoff filter ($\lambda > 400$ nm) were obtained from Sigma Koki Co. Ltd., and were located between the light source and the sample reactor. The UV–vis light source was a Toshiba 75-W Hg lamp (irradiance, ca. 0.3 mW cm^{-2}; maximal emission, 360 nm) and was positioned in the microwave set-up such as to irradiate the sample reactor through the hole on the side of the waveguide.

2.3. Chemicals and photodegradation procedures

High-purity grade 4-chlorophenol (4-CP) was purchased from Wako Pure Chemical Industries Ltd. Aqueous 4-CP solutions (30 mL; concentrations either 0.020 mM, or 0.050 mM or 0.10 mM) were introduced into a high-pressure 150-mL Pyrex glass cylindrical reactor (maximal pressure, 1.5 MPa) along with the TiO_2 powdered samples (loading, 5 mg or 60 mg). The concentrations of 4-CP and loading level of the TiO_2 specimens were chosen such that the reaction times under microwave irradiation were reasonable. For instance, when the photodegradation of 4-CP was carried out with 60 mg of P-25 TiO_2 and 0.10 mM of 4-CP the reaction was over in less than 10 min, making it difficult to measure the temperature rise such as that shown in the inset of Fig. 1. Accordingly, in this case the TiO_2 loading was decreased to 5 mg.

To the extent that our principal goal was to assess the microwave specific effect in dispersions involving nitrogen-doped TiO_2 systems, the reaction dynamics of 4-CP were an important parameter. The temperature of the photodegradation of 4-CP in aqueous dispersions (TiO_2/photo method) was near-ambient (25–30 °C), whereas the temperature was 114 °C for the microwave-assisted (MW) and thermally assisted (CH) photodegradation processes.

Three different approaches were chosen to achieve the decomposition of 4-chlorophenol, to examine its dynamics, and to assess

the microwave effects. The first approach in the photoassisted degradation of 4-CP involved irradiation of the TiO_2 dispersions by UV alone, or by vis radiation alone, or by UV–vis light in combination with microwave irradiation (i.e. UV/MW, vis/MW, and UV–vis/MW, methods). In the second approach, the photodegradation of 4-CP was followed under light irradiation alone (viz. UV–vis, UV and vis methods), whereas in the third case the photoassisted degradation of 4-CP was thermally assisted using externally applied conventional heat (UV–vis/CH, UV/CH and vis/CH methods). In the latter approach the external heat was supplied by coating one part of the cylindrical photoreactor with a metallic film (MOCVD technique) on one side at the bottom of the reactor (applied voltage ≤100 V). The uncoated side was used to permit light irradiation through to the reactor. The rate of increase of temperature (error, ca. ±1 °C) and pressure in the combined conventional heating/light irradiation methods were maintained at levels otherwise identical to those used for the combined microwave/light irradiation methods. No differences were observed in the temperature profiles using either microwave generated heat or conventional heating.

The time profiles of the degradation of 4-CP were obtained by monitoring the concentration changes of 4-CP by UV–vis spectroscopy on a JASCO liquid chromatograph (HPLC) equipped with a JASCO UV-2070 UV–vis diode array and a multi-wavelength detector; the column was a JASCO Crestpak C-18S. The eluent consisted of a mixed solution of methanol/water (1:2, v/v ratio).

2.4. Temperature measurements and dielectric parameters of TiO_2 powders

For these experiments the temperatures of the TiO_2 powders were measured using an Anritsu Meter Co., Ltd. FL-2000 fiber optic thermometer in a commercial multimode microwave chemical apparatus device (Tokyo Rikakikai Co. Ltd., MWO-1000S system). The TiO_2 powder samples were packed in the tube reactor (diameter, 8 mm) set up in the multimode microwave applicator, with the fiber optics thermometer positioned at the center of the packed TiO_2 powder; the positions of the thermometer and reactor were maintained constant throughout. The temperature profiles were recorded at 5-s intervals. Temperature measurements were performed twice; variations between readings were negligible. Dielectric constants (ε_r') and dielectric loss factors (ε_r'') of the TiO_2 powders contained in the quartz tube were analyzed by the perturbation method using the TEM_{010} (transverse electric wave) mode of the cylindrical cavity resonator. The measured dielectric factors consisted of those for air and TiO_2 powder combined. The proportion of TiO_2 in the quartz tube was calculated by the weight of the TiO_2 powder and the density (g cm^{-3}) determined for each TiO_2 powder using the Quantachrome Ultra Pycnometer 1000.

2.5. In situ Raman spectroscopy of TiO_2 samples

The microwave effects (thermal or non-thermal) on the metal-oxide specimens were probed using an in situ laser Raman microscopic system (JASCO Co., NRS-5100; excitation wavelength, 785 nm so as to avoid photon absorption by the N-doped samples) in combination with an assembled microwave irradiation applicator as illustrated in Fig. 2. The TiO_2 powder (loading, 0.10 mg) was placed on the copper dish (ϕ = 8 mm) in the microwave applicator. Continuous microwave irradiation was achieved through the BNC cable (Bayonet–Neil–Concelman) using a 2.45-GHz microwave semiconductor generator (Fuji Electronic Industrial Co. Ltd.; GNU-201AA) that can be operated at a maximal power of 200 W. The actual microwave power used was 72.2 W, sufficient to irradiate the quantities of TiO_2 samples. The incident microwaves irradiating the TiO_2 powders on the copper dish were monitored with a 2.45-GHz microwave electric field sensor equipped with a Schottky diode (Fuji Electronic Industrial Co. Ltd.). Raman spectra were recorded through a microscope through the hole (ϕ = 7.8 mm) in the microwave apparatus. Temperature changes of the TiO_2 powders were monitored with a radiation thermometer. *In situ* recording of the Raman spectra was carried out under microwave irradiation both in the dark (MW/dark method) and under simultaneous microwave and UV irradiation (MW/UV method). The incident UV light was obtained from a fluorescent lamp (irradiance, ca. 0.3 μW cm^{-2} at 360 nm) through the hole on the cover of the microwave applicator. The specimens were microwave-irradiated at 1-min intervals. Measurements under microwave irradiation were continued for 7 min. Exploratory experiments determined that the error margins in peak intensities of the Raman bands for the TiO_2 specimens in the absence of MW and UV irradiation were ≤2.5%.

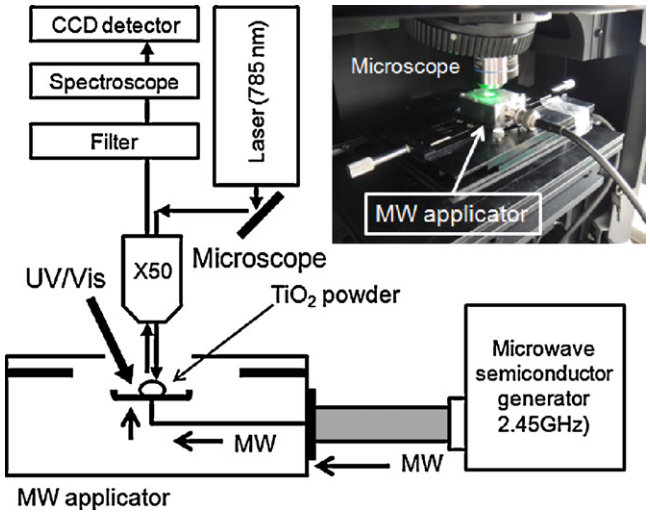

Fig. 2. Experimental setup for the *in situ* Raman spectroscopy of TiO_2 powdered specimens using an integrated microwave and UV–vis radiation system.

3. Results and discussion

3.1. Properties of undoped and nitrogen-doped TiO_2 specimens

The band-gap energy of undoped Degussa P-25 TiO_2 determined by diffuse reflectance spectroscopy (DRS) was 3.19 eV – see Table 1 – and represents the absorption edge in excellent accord with 3.2 eV noted in Degussa's data sheet for the sample. The absorption edge of N-doped P-25 powder (denoted N-P25 TiO_2) was 0.2 eV lower at 3.00 eV. We wish to emphasize that the latter value represents the *extrinsic* and not the *intrinsic* band-gap energy of doped TiO_2 samples as too often incorrectly claimed by many (see e.g. references in the reviews by Serpone et al. [13,14]). In the case of undoped ST-01 TiO_2, the band-gap energy determined by DRS was 3.21 eV, whereas the absorption edge of the nitrogen-doped N-ST01 TiO_2 sample shifted down to 3.10 eV.

Nitrogen doping of the TiO_2 particles increased the size relative to undoped TiO_2 systems, most significant for the ST-01 sample. Such increase in particle size can lead [15] to a significant, albeit non-linear decrease in the surface area of the N-doped TiO_2 samples, and to an increased number of color centers (e.g. Ti^{3+}; ESR measurements [20]). The nitrogen content in N-doped TiO_2 particles (<6.1% for N-P25 TiO_2 and 0.81% for the N-ST01 analog) was estimated by energy dispersive X-ray spectroscopy (EDS) using a Hitachi High-Technologies Co. H-7650 transmission electron microscope. The level of anatase in the N-doped P25 particles remained essentially the same, whereas it increased slightly for the N-doped ST-01 TiO_2 particles.

Table 1
Band-gap energy, BET surface area, quantity of anatase and particle size of naked TiO_2 powder (P-25 and ST-01), and nitrogen-doped TiO_2 (N-P25 and N-ST01) specimens.

TiO_2 sample act	Band-gap (eV)	Surface area ($m^2\ g^{-1}$)	Particle size (nm)[a]	Crystallite size (nm)[b]	Anatase (wt.%)
P-25	3.19[c]	56	23	17	81
N-doped P25	3.00[d]	41	32	20	80
ST-01	3.21[c]	304	4	7	93
N-doped ST01	3.10[d]	96	17	16	97

[a] By TEM.
[b] By XRD using the (101) peak for anatase.
[c] Intrinsic band-gap of undoped TiO_2 specimens.
[d] Apparent or extrinsic band-gap of N-doped TiO_2 specimens.

3.2. Dielectric properties of N-doped TiO_2 powders on absorption of microwaves

The thermal behavior of solids on absorption of microwaves can be assessed by determining the temperature–time profiles as performed for undoped TiO_2 and N-doped TiO_2 powdered samples and displayed in Fig. 3. For the undoped P-25 TiO_2 and undoped ST-01 samples the temperatures reached were 57.9 °C and 79.6 °C, respectively on absorption of 200-W microwaves for 180 s of irradiation. By contrast, the temperature reached by the N-doped sample N-P25 TiO_2 powder was 93.8 °C and for the N-ST01 sample 87.1 °C. Clearly, microwave heating efficiencies improved by nitrogen doping the metal oxides. Estimated heating rates were 0.178 °C s^{-1} mg^{-1} for P-25, 0.389 °C s^{-1} mg^{-1} for N-P25, 0.311 °C s^{-1} mg^{-1} for ST-01, and 0.343 °C s^{-1} mg^{-1} for N-ST01. Thus, the increased rates of temperature on nitrogen doping were 2.2-fold greater (i.e. ca. 120% faster) for N-P25 relative to undoped P-25, and ca. 10% faster for the N-ST01 sample relative to undoped ST-01 TiO_2. Thus nitrogen doping of P-25 TiO_2 enhanced the heating effect of the microwaves to a greater extent than did nitrogen doping of the ST-01 sample. The data variations suggest that the enhanced heating of the N-P25 TiO_2 was likely caused by selective heating at nitrogen dopant sites within the lattice and at the surface of the particles (also see below). In this regard, an earlier study [9] showed that a H_2-treated (reduced) P-25 TiO_2 powder displayed a greater increase of temperature on microwave irradiation than did untreated P-25, which caused different effects on the electronic characteristics of the H_2-treated *vis-à-vis* untreated TiO_2 particles. It was inferred that such temperature variations were caused by the occurrence of further oxygen vacancies in the H_2-treated metal oxide that led to changes in the electronic properties of TiO_2 specimens and thus to changes in the heating efficiency of the microwaves. Related to this inference, the heating of titanium oxides TiO_{2-x} ($x > 0$) bearing oxygen defects (i.e. oxygen vacancies (V_Os)), which lead to the appearance of spontaneous magnetization, was shown to be enhanced by the microwaves' magnetic field [21].

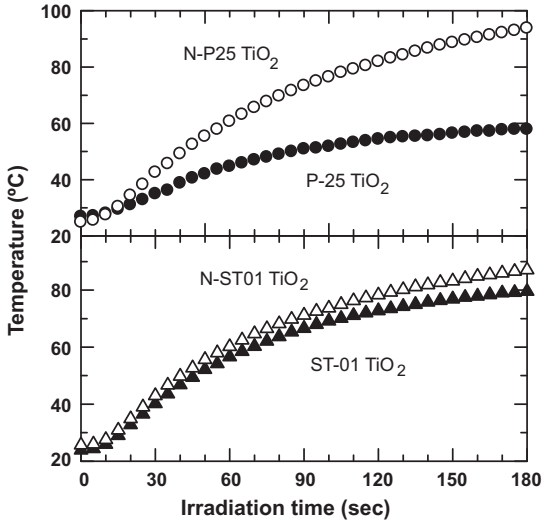

Fig. 3. Temperature–time profiles of undoped TiO_2 and nitrogen-doped TiO_2 powdered samples subjected to microwave irradiation. Upper graph: solid circles (●), P-25 TiO_2; open circles (○), N-P25 TiO_2. Lower graph: open triangles (△), N-ST01 TiO_2; solid triangles (▲), ST-01 TiO_2.

Germane to the present discussion, Di Valentin et al. [22] reported that N-doping of TiO_2 leads to a substantive reduction of the energy of formation of oxygen vacancies V_Os (from 4.3 eV to 0.6 eV for anatase) with important consequences in the generation of *F*-type and Ti^{3+} color centers. Substitutional N-doping can be stabilized by the presence of oxygen vacancies ($N_{S-O} + V_O$) under oxygen-poor experimental conditions, whereas under oxygen-rich conditions interstitial N species (N_I) are favored [23]. Accordingly, the results shown in the upper graph of Fig. 3 suggests that, contrary to the undoped P-25 TiO_2 specimen, the nitrogen-doped N-P25 TiO_2 sample contains additional oxygen vacancies and that part of the microwave radiation is thus consumed at oxygen vacancies and at N dopant surface and lattice sites. Accordingly, microwave irradiation generates non-equilibrium heating of the N-P25 sample, whose occurrence on a solid surface was also encountered by Sato and Tanaka [24] who reported a rate of temperature increase of 0.311 °C s^{-1} mg^{-1} in a heavily doped N-P25 TiO_2 system (16 wt.% nitrogen) by microwave irradiation in contrast to 0.389 °C s^{-1} mg^{-1} for a N-P25 TiO_2 sample that contained only ca. 6 wt.% nitrogen. Evidently, the heating efficiency of the microwave radiation does not increase linearly upon continued nitrogen doping in the P-25 TiO_2 system as such a doped system is likely no longer N-doped TiO_2 but a product better described as a titanium oxynitride possessing entirely different electronic and structural characteristics. While there is a considerable change in the rate of temperature increase for the P-25 TiO_2s, the same is not the case for the ST-01 TiO_2 system whereupon nitrogen doping seems to have little, if any, effect in the heating efficiency of the microwaves (Fig. 3).

Dielectric loss factors (ε_r'') and dielectric constants (ε_r') of undoped P-25 and ST-01 samples, and nitrogen-doped N-P25 and N-ST01 TiO_2 powders were determined at a microwave frequency of 2.45 GHz (Table 2). Recall that the dielectric loss factor is a measure of the efficiency with which the electromagnetic energy of microwaves is converted to heat. As we saw above, the heating rate by microwaves on nitrogen doping the P-25 TiO_2 nanoparticles showed a remarkable increase, although the dielectric loss factor is lower than for the undoped P-25 specimen. For undoped ST-01 and nitrogen-doped N-ST01 samples the corresponding dielectric loss

Table 2
Dielectric loss factors (ε_r'') and dielectric constants (ε_r') at the 2.45-GHz microwave frequency for undoped P-25 and ST-01 samples, and for N-doped N-P25 and N-ST01 TiO_2 specimens.

TiO_2 specimen	Dielectric loss factor (ε_r'')	Dielectric constant (ε_r')
P-25	0.283	10.48
N-P25	0.226	18.73
ST-01	0.482	8.63
N-ST01	0.429	10.38

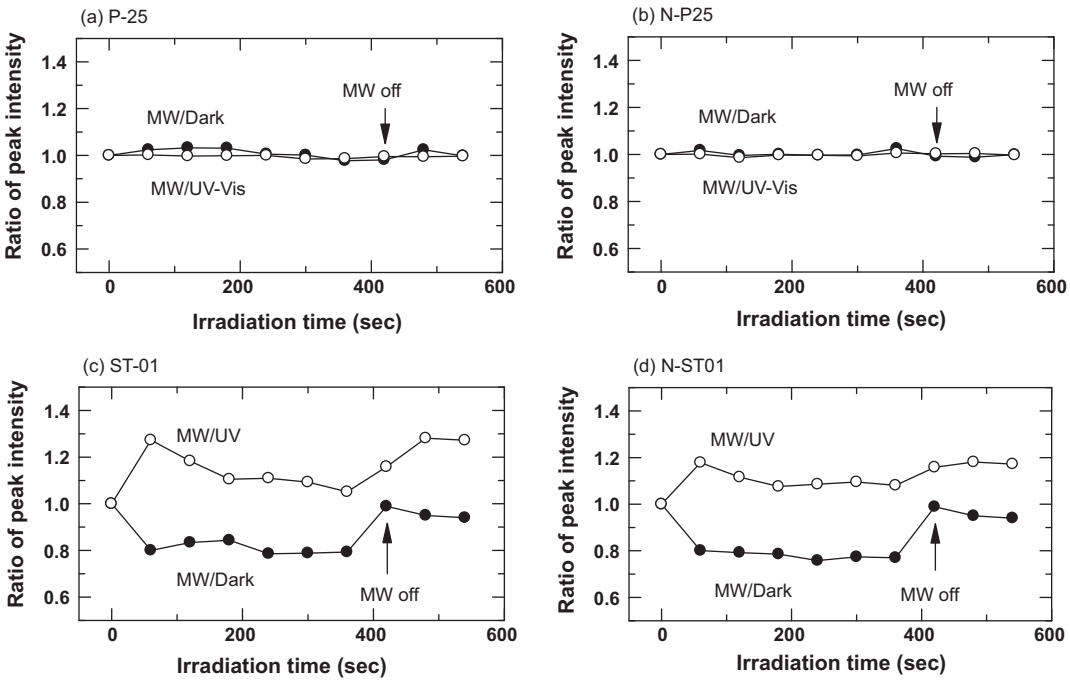

Fig. 4. Time variations in the peak intensity ratios in the Raman spectra of the P-25, N-P25, ST-01 and N-ST01 TiO_2 powdered specimens under microwave irradiation with dark- and UV-irradiation conditions. Ratios were calculated relative to the bands of the initial titania specimens observed at 143 cm^{-1} for the undoped P-25 and doped N-P25 TiO_2 samples, and at 144 cm^{-1} for the undoped ST-01 and for the doped N-ST01 TiO_2 specimens.

factors (ε_r'') were 0.482 and 0.429, respectively, again a lower ε_r'' for the N-doped sample. By contrast, the dielectric constants (ε_r') of N-P25 and N-ST01 increased with nitrogen doping. In both cases, the heating efficiency of the microwaves did not follow the respective differences in dielectric loss factors (ε_r''), and even though nitrogen doping increased the relative permittivity of the metal-oxide samples, there are no relationships between heating efficiencies (Fig. 3) and dielectric constants (ε_r'; Table 2).

The divergences in the temperature–time profiles cannot be ascribed to dielectric losses in the solids. However, though conduction losses in solids are small at ambient temperatures, they can increase substantially with increase in temperature as evidenced for alumina (Al_2O_3), for which dielectric losses are negligibly small (ca. 10^{-3}) at room temperature but can reach fusion within a few minutes in a microwave cavity [3]. Such effect originates from a strong increase of conduction losses associated with the thermal activation of electrons within the lattice which migrate from the oxygen 2p valence band to the 3s3p conduction band of alumina. Conduction losses in solids are enhanced by the presence of defects, which tend to reduce the effective energy gap of the solid, i.e. defect levels within the intra-gap afford the solid with an apparent or *extrinsic* band gap as opposed to the *intrinsic* valence-conduction band gap [13,14,23].

3.3. *In situ Raman spectroscopy and optical phonons in TiO_2*

Fairly strong Raman-active vibrational modes of the TiO_2 specimens were observed at 143–144 cm^{-1} ($E_g^{(1)}$), 395–396 cm^{-1} (B_{1g}), 516–517 cm^{-1} ($A_{1g} + B_{1g}$), and 637–639 cm^{-1} ($E_g^{(2)}$) in good accord with the Raman spectral band positions assigned previously by Balachandran and Eror [25] to pure anatase and by Liu et al. [26] to nitrogen-doped TiO_2. Fig. 4 illustrates the changes of the intensity of the most intense 143–144 cm^{-1} Raman spectral bands ($E_g^{(1)}$) of each TiO_2 specimen subjected to MW/dark and MW/UV irradiation relative to the intensities of the corresponding bands in the non-irradiated samples. We hasten to point out that the intense $E_g^{(1)}$ band displayed no broadening, so that phonon [27] confinement and other factors [28–31] that typically lead to band broadening were of no consequence in the present case.

For undoped P-25 and N-P25 TiO_2 samples, it is evident that no changes in the Raman peak intensities occurred when subjecting the TiO_2 samples to either microwaves or to UV–vis radiations or to both. The influence of microwaves on the Raman spectral features of P-25 and N-P25 TiO_2 samples was rather inconsequential. As evidenced by the data of Fig. 3, the heating efficiency of P-25 TiO_2 was enhanced on nitrogen doping, yet the Raman spectrum of the N-doped TiO_2 (N-P25) specimen showed no variations. By contrast, the Raman intensities of the 144 cm^{-1} peak for undoped ST-01 TiO_2 and for the nitrogen-doped N-ST01 TiO_2 sample initially increased on simultaneous absorption of microwaves and UV–vis radiation (MW/UV), subsequent to which the peak intensities tended to decrease with continued irradiation. This clearly establishes the impact of microwaves on the ST-01 and N-ST01 TiO_2 samples, contrary to a non-absorber of microwave radiation such as a quartz crystal (SiO_2), which showed neither changes in peak intensities nor shifts of the Raman spectral bands. Peak intensities (Fig. 4c and d) returned to their UV–vis positions (time, 60 s) on termination of microwave irradiation. However, in the absence of UV–vis radiation (MW/dark), the peak intensities decreased significantly when the ST-01 and N-ST01 specimens were subjected to microwave radiation alone, after which they returned to their initial values (time, 0 s) on termination of microwave irradiation.

The intensity of a Raman spectral band is proportional to the molecular density N and to the polarizability α as expressed in Eq. (1) [32]:

$$\text{intensity} \approx N\alpha^2 \approx N\left\{\left(\frac{\delta\alpha}{\delta Q}\right)_0 Q\right\}^2 \quad (1)$$

where Q denotes the normal coordinates. Taking that no changes in molecular density occurred when the TiO_2 samples were subjected to microwave radiation, changes in peak intensities may

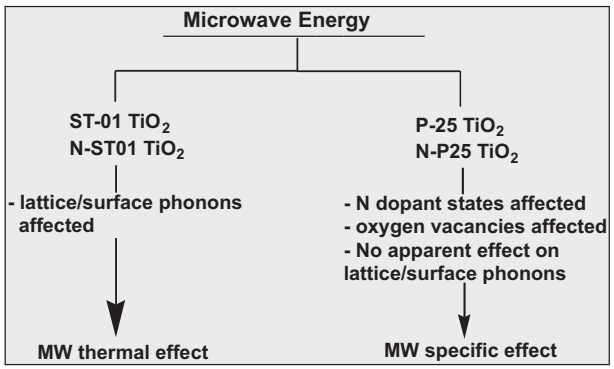

Scheme 1. Consumption of microwave electromagnetic energy in undoped P-25 TiO_2 and ST-01 TiO_2 samples, and in nitrogen-doped N-P25 TiO_2 and N-ST01 TiO_2 specimens.

then be related to the changes in the polarizability of the TiO_2 crystalline particle. For undoped and nitrogen-doped P-25 TiO_2 (N-P25) samples the polarizability remained invariant under microwave irradiation, inferring that the absorbed microwave energy was likely used to affect the nitrogen dopant sites and oxygen vacancies. By comparison, the polarizabilities, and thus surface phonons, in the ST-01 and N-ST01 specimens are significantly affected (decrease) by the microwaves and UV–vis radiation (Scheme 1). The microwaves were of no consequence to the vibrational modes (phonons) in undoped P-25 and doped N-P25 TiO_2 nanoparticles (see also Fig. 4a and b).

Fluctuations in the polarizability of a crystal with rocksalt structure by added impurities in the lattice have been shown [33] to induce a non-vanishing first-order electronic polarizability giving rise to a first-order Raman scattering of light that was analyzed by Raman scattering spectroscopy. In keeping with this notion, we infer that the decrease in the polarizabilities of ST-01 and N-ST01 samples caused the decrease in the intensities of the lattice/surface phonon bands. Microwave phonon transmission properties in solids, e.g. rutile TiO_2, at ambient temperatures have been of interest for some time [34]. Optical phonon band intensities decreased in ST-01 and N-ST01 TiO_2 specimens under microwave irradiation, whereas those of P-25 and N-P25 TiO_2 specimens showed no variations with irradiation time under otherwise identical conditions (Fig. 4a and b). Optical near-surface phonons in the (1 1 0) TiO_2 crystal face have been observed in this wide band-gap metal oxide by Raman spectroscopy [35]. However, such optical phonons might not correlate directly with enhancement of photoactivity of TiO_2 samples influenced by a microwave specific effect. Riobóo et al. [36] examined acoustic and optical phonons of TiO_2 embedded in a polymer matrix in the 15–20 GHz range for possible use of the matrix in the elimination of foodstuff pathogens. In the present context, consumption of microwave energy in TiO_2 samples through excitation of acoustic phonons is not precluded by our current results. In this regard, possible relationships between acoustic phonons, local microwave energy expenditure, and the photoactivity of TiO_2 samples will be the subject of a future investigation.

The dynamics of microwave-/photo-assisted degradation of bisphenol A (BPA) in aqueous P-25 TiO_2 dispersions improved dramatically under ambient temperature conditions, which inferred that the microwave radiation is not a simple heat source [37]. When the microwave energy in TiO_2 is consumed as heat by the lattice/surface vibrations (microwave-induced phonons) of the crystalline particles, no microwave specific effect is clearly evident. Moreover, changes in lattice/surface vibrations induced by absorption of microwave energy appear to be of no consequence to the photoactivity of P-25 TiO_2. On the other hand, the photoactivity of P-25 TiO_2 particles improves because the microwave energy affects local defect sites to a greater extent than lattice/surface phonons for this particular metal-oxide sample.

To the extent that the photo-assisted and microwave-assisted degradation of an organic substrate might provide a key parameter to delineate between microwave thermal and non-thermal effects, it was important to examine the degradation of 4-chlorophenol under UV, MW, and UV/MW irradiation.

3.4. Microwave- and photo-assisted degradation of 4-CP in aqueous media

The time profiles of the degradation of aqueous 4-CP solutions are displayed in Fig. 5(a-i to a-iv) for undoped P-25 TiO_2 and nitrogen-doped N-P25 TiO_2. Fig. 5(b-i to b-iv) displays the results for undoped Ishihara ST-01 and doped N-ST01 TiO_2 samples under various conditions. The corresponding dynamics are summarized in Table 3 [38].

3.4.1. The P-25 TiO_2 system (a-(i–iv))

The UV–vis photodegradation dynamics of aqueous 4-CP were enhanced considerably (ca. 3-fold faster) with concomitant irradiation by microwaves (UV–vis/MW) due, in part, to the higher temperature (114 °C) generated by microwave heating (Fig. 5(a-i)). However, under otherwise identical temperatures, obtained by conventional heating (resistance heating of coated electrode on reactor surface), the UV–vis photodegradation of 4-CP by UV–vis/CH irradiation was 2-fold slower. For N-P25 TiO_2, the UV–vis photodegradation of aqueous 4-CP (pH = 5.8) was enhanced significantly in all three cases (i.e. with no MW, with MW, and with CH heating) relative to undoped P-25 TiO_2 (Fig. 5(a-ii)). Using only UV radiation to activate the N-P25 TiO_2 sample, the photoassisted degradation rate increased 2-fold relative to undoped TiO_2; vis irradiation showed a behavior similar to UV irradiation in the absence of microwaves and conventional heating (compare rows a-iii and a-iv for column 4 in Table 3).

With microwave irradiation or with conventional heating, the photodegradation process was also accelerated somewhat (columns 5 and 6 vs. column 4). Interestingly, the degradation of 4-CP (column 4) photoassisted by vis radiation was enhanced relative to the UV-activated N-P25 TiO_2 but otherwise little variation was observed relative to the UV–vis activated nitrogen-doped sample. With conventional heating the photodegradation dynamics decreased when using vis radiation alone. Overall, comparison of columns 5 and 6 of Table 3 demonstrates that conventional heating was significantly less effective in driving the photodegradation, irrespective of whether or not P-25 TiO_2 was nitrogen-doped. A microwave specific effect appears to be determinant only for the N-P25 TiO_2 irradiated by vis light and for the UV–vis irradiated undoped P-25 TiO_2 dispersions.

3.4.2. The N-ST01 TiO_2 (b-(i–iv))

Comparison of row a-i with row b-i in Table 3 reveals that undoped Ishihara ST-01 TiO_2 was more photoactive (8-fold) toward the photodegradation of aqueous 4-CP than was undoped Degussa P-25 TiO_2. Regardless of the conditions used (with and without MW, and light irradiation) the nitrogen-doped N-ST01 TiO_2 was considerably less photoactive than its undoped counterpart. Even more significant, the photodegradation dynamics with N-ST01 TiO_2 displayed little variations (if any) across rows b-(ii–iv) and columns 4–6. Conventional heating (thermal effects) and microwave irradiation (thermal and non-thermal effects) were of no consequence in the photodegradation of 4-CP in this case. In fact, for this metal-oxide sample no microwave specific effects are apparent, and neither are MW and CH thermal effects.

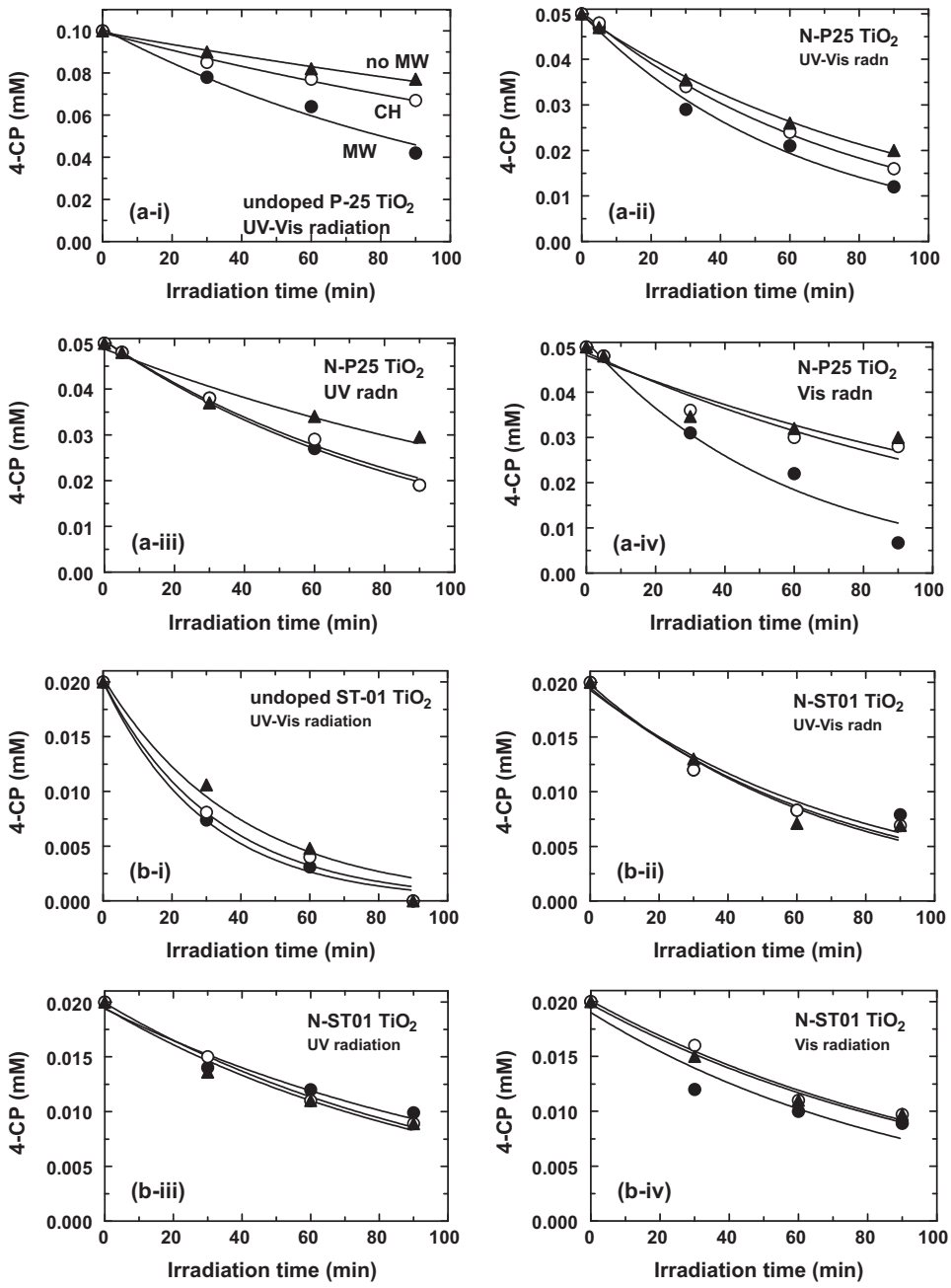

Fig. 5. Time profiles of the photodegradation of 4-CP (a-i: 0.10 mM; a-ii, a-iii, a-iv: 0.050 mM; b: 0.020 mM) in aqueous media with (a-i) undoped P-25 TiO_2, (a-ii, a-iii, a-iv) nitrogen-doped P-25 TiO_2; (b-i) undoped ST-01 TiO_2, (b-ii, b-iii, b-iv) nitrogen-doped ST-01 TiO_2 under UV/vis irradiation (i and ii), under UV irradiation only (iii), and under vis irradiation alone (iv). Solid triangles (▲) with TiO_2 present and irradiation with UV–vis, or UV, or vis wavelengths (the TiO_2/photo method). Solid circles (●) with TiO_2 present and irradiation with microwaves (MW) together with UV–vis radiation, or UV radiation, or vis radiation (the TiO_2/photo/MW method); open circles (○) thermally assisted photodegradation in the presence of TiO_2 irradiated with UV–vis wavelengths, or UV wavelengths, or vis wavelengths (the TiO_2/photo/CH method).

Table 3
First-order rate constants (10^{-2} min^{-1}) for the degradation of 4-CP using the undoped P-25 TiO_2 and N-doped P-25 TiO_2 (N-P25), and the undoped ST-01 TiO_2 and N-doped ST-01 TiO_2 (N-ST01) by the TiO_2/photo, TiO_2/photo/MW and TiO_2/photo/CH methods.

Specimen	Fig. 5	Radiation (photo)	k_{deg}[a] (photo)	k_{deg}[a] (photo/MW)	k_{deg}[a] (photo/CH)
Undoped P-25 TiO_2	a-i	UV–vis	0.30 ± 0.02	0.88 ± 0.09	0.44 ± 0.03
N-P25 TiO_2	a-ii	UV–vis	1.05 ± 0.03	1.58 ± 0.10	1.27 ± 0.03
	a-iii	UV	0.61 ± 0.09	1.05 ± 0.04	1.00 ± 0.06
	a-iv	Vis	0.64 ± 0.14	1.70 ± 0.22	0.73 ± 0.11
Undoped ST-01 TiO_2	b-i	UV–vis	2.53 ± 0.43	3.36 ± 0.28	3.03 ± 0.35
N-ST01 TiO_2	b-ii	UV–vis	1.42 ± 0.21	1.25 ± 0.24	1.35 ± 0.17
	b-iii	UV	0.95 ± 0.11	0.81 ± 0.12	0.94 ± 0.04
	b-iv	Vis	0.88 ± 0.08	1.03 ± 0.24	0.87 ± 0.09

[a] Rate constants: 10^{-2} min^{-1}.

3.5. Nitrogen-doping and the UV or vis photoassisted process under microwave irradiation

Second generation metal-oxide photocatalysts, or otherwise so-called visible-light-active (VLA) TiO_2 systems doped with nitrogen possess, in most cases, attractive features toward the photooxidation of organic and inorganic (e.g., NO_x) substrates [13]. Orlov et al. [39] have suggested that visible light activity of N-doped TiO_2 cannot be attributed solely to the effect of nitrogen-doping and other effects; creation of (additional) oxygen vacancies may be a significant consequence of the doping process. The simultaneous presence of N dopants and oxygen vacancies, V_Os, can also lead to charge transfer states (reaction (2); F and F^+ are color centers) that can further contribute to the visible-light photoactivity [13,14].

$$V_O(F) + N \rightarrow V_O^{\bullet}(F^+) + N^- \quad (2)$$

Chen et al. [40] placed the energy levels of F-type color centers at energies of 0.87 eV (F), 1.78 eV (F^+) and 0.20 eV (F^{2+}) below the bottom level of the conduction band.

In a recent related article, Kuznetsov and Serpone [23] concluded that the various DRS spectral observations reported thus far strongly infer that the absorption bands (denoted AB1, AB2, and AB3) of cation- and anion-doped TiO_2 systems in the 400–600 nm spectral region, which impart visible-light photoactivity to nearly all doped TiO_2 specimens, originate from F-type color centers associated with oxygen vacancies. Spectral features at wavelengths longer than ca. 600 nm (i.e., at $h\nu < 2.0$ eV) were attributed to Ti-related color centers. Emeline et al. [41] described a model that rationalizes the stabilization of color centers and proposed different mechanisms for the physical relaxation of the N-doped TiO_2s electronic subsystem and for the chemical pathways when a N-doped metal oxide is subjected to UV-light or to visible-light irradiation.

The influence of microwaves on the doped N-P25 TiO_2-photoassisted processes under UV and vis light irradiation is schematically illustrated in Scheme 2.

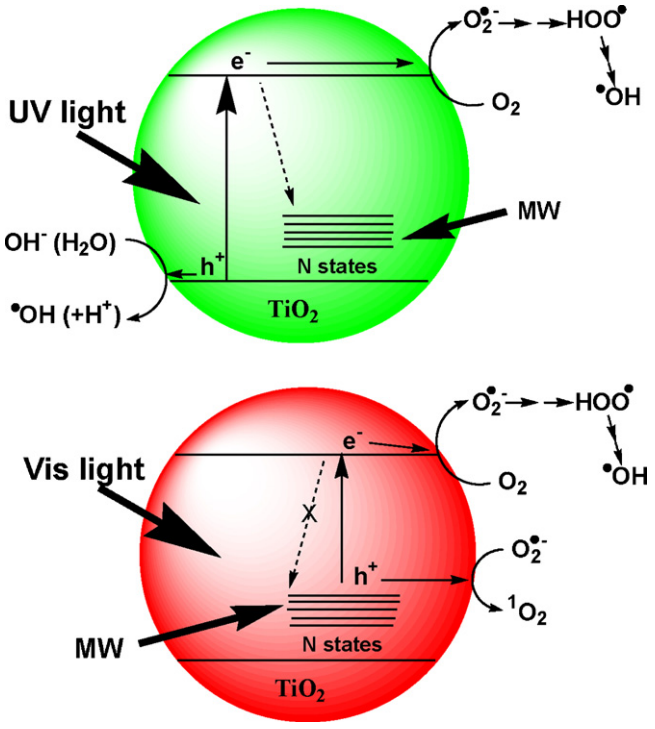

Scheme 2. Cartoon displaying the influence of microwaves in the photoassisted process for nitrogen-doped N-P25 TiO_2 under ultraviolet (UV) light and visible (vis) light.

3.5.1. The UV irradiation case

Absorption of UV light by N-doped TiO_2 particles of energy greater than band gap (ca. 3.19 eV, onset of absorption λ = 388.4 nm) generates electron–hole pairs. Holes (h^+) are ultimately trapped by surface HO^- ions or by adsorbed H_2O molecules on the particle surface yielding $^{\bullet}OH$ radicals (and H^+), whereas concomitant scavenging of conduction band electrons (e^-) by surface-adsorbed O_2 molecules yield superoxide radical anions, $O_2^{\bullet -}$, which on protonation generate the $^{\bullet}OOH$ radicals and ultimately additional $^{\bullet}OH$ radicals. As evidenced by the temperature rise of Fig. 3 (upper graph), the microwave energy in part heats the ensemble of N-P25 particles (more so than undoped P-25 TiO_2) and in part is expended on the N states. The photodegradation dynamics of 4-CP ($1.05 \pm 0.04 \times 10^{-2}$ min^{-1}) under UV/MW irradiation and under UV/CH irradiation ($1.00 \pm 0.06 \times 10^{-2}$ min^{-1}) reported in Table 2 indicate that microwaves display only a thermal effect under these conditions. The presence of intra-gap N states in N-P25 TiO_2 nanoparticles are inconsequential to the photodegradation process, inasmuch as the corresponding dynamics relative to undoped P-25 are nearly identical within experimental error ($0.88 \pm 0.09 \times 10^{-2}$ min^{-1} vs. $1.05 \pm 0.04 \times 10^{-2}$ min^{-1}, respectively). Alternatively, even though the microwaves' role may also be non-thermal, the latter microwave-assisted photodegradation dynamics may be subdued by the presence of the N states as these states may inhibit the photoassisted reaction by acting as electron traps and as recombination centers [13,14,22], thereby inhibiting formation of $O_2^{-\bullet}$ and $^{\bullet}OH$ radicals. The influence of oxygen vacancies in the photodegradation process is not precluded as the microwaves can also impact these lattice and surface defects, not least of which is the role that oxygen vacancies can play as electron traps.

3.5.2. The vis irradiation case

N-doped TiO_2 materials typically display absorption features and absorption edges red-shifted to the visible spectral region. However, photoactivity of visible-light-active (VLA) systems under vis irradiation has not always correlated with absorption features. Tachikawa et al. [42] addressed this issue and described some of the mechanistic features of photoactive VLA TiO_2 specimens. Solid-state NMR and transient diffuse reflectance (TDR) spectroscopy led them to deduce that photoassisted oxidations of organic compounds occurring on the surface of nitrogen-doped TiO_2 ($TiO_{2-x}N_x$) involve surface intermediates generated from oxygen reduction, i.e. $O_2^{-\bullet}$ radical anions, or otherwise water oxidation yielding $^{\bullet}OH$ radicals, rather than photogenerated holes (h^+) as these may be trapped at intra-gap N states (Scheme 2). Their work [42] inferred two conditions that must be met for advanced visible-light-active TiO_2-based photocatalysts: (a) appropriate lower-energy photo-thresholds for visible-light absorption, and (b) high carrier mobilities.

Absorption of vis radiation by N-doped samples also generates conduction band electrons, albeit the photogenerated holes are now part of the intra-gap dopant localized states with a lesser oxidation potential than holes in undoped P-25 TiO_2 [15]. Direct and indirect trapping of electrons by F^+ and F^{2+} color centers are also likely to occur. Despite the negligible anodic shift of the N-doped TiO_2 conduction band level relative to undoped TiO_2 suggested by Sakthivel and Kisch [43], electron reduction of molecular oxygen [44] and formation of $^{\bullet}OOH$ radicals with ultimate formation of $^{\bullet}OH$ radicals through prior generation of H_2O_2 can occur by a pathway not dissimilar to the pathway under UV irradiation of the doped samples (Scheme 2). Moreover, during vis irradiation of N-doped TiO_2, the superoxide radical anion $O_2^{-\bullet}$ can be oxidized by holes of the N dopant states to yield singlet oxygen, $^1O_2$, as recent EPR spin-trapping measurements by Rengifo-Herrera et al. [45] have shown who proposed that formation of $^1O_2$ is thermodynamically favored

under visible light irradiation through a mechanism that involves $O_2^{-\bullet}$ in a manner not unlike that reported by Daimon et al. [46] for the production of $^1O_2$ on undoped P-25 TiO_2 albeit under UV illumination. Oxidation of $O_2^{-\bullet}$ to produce $^1O_2$ necessitates only a redox potential of 0.34 V (vs. NHE) [47], so that its formation from superoxide radical anion oxidation by localized N dopant holes is not an unlikely event.

The influence of microwaves on N dopant states when doped N-P25 TiO_2 is irradiated simultaneously with vis radiation, as attested by comparing the photodegradation dynamics of 4-CP under vis/MW, as opposed to vis/CH irradiation ($1.70 \pm 0.22 \times 10^{-2}\,min^{-1}$ vs. $0.73 \pm 0.11 \times 10^{-2}\,min^{-1}$; Table 3), indicates a possible microwave specific effect under these conditions; i.e. non-equilibrium heating promotes the photoactivity of the doped specimen. By contrast, a similar specific effect by the microwaves is mooted for the N-ST01 TiO_2 sample as the photodegradation dynamics are similar, within experimental error, across all the experimental conditions (see Table 3) and this even for undoped ST-01 TiO_2.

4. Concluding remarks

This article examined the characteristics of microwave radiation on two first generation undoped and second generation nitrogen-doped TiO_2 nanomaterials (Degussa P-25 TiO_2; Ishihara ST-01 TiO_2). Band gaps of undoped samples accorded with previously reported values, whereas the apparent (i.e. *extrinsic*) band gaps of N-doped samples were of lower energy as expected on introducing intra-gap N states. The sizes of TiO_2 particles following N doping increased somewhat; BET surface areas diminished. Dielectric constants and dielectric loss factors were determined with 2.45-GHz microwaves. Temperature–time profiles measured for all four samples showed that the efficiency of microwave heating N-doped specimens was greater, and was particularly significant for the N-doped P25 sample but negligibly small for the ST-01 samples. *In situ* Raman spectra, recorded during microwave irradiation and with and without UV–vis irradiation, revealed a negligible microwave effect on surface optical phonons for undoped P-25 and N-P25 TiO_2 systems, contrary to Ishihara ST-01 and N-ST01 TiO_2 samples for which microwave irradiation showed significant changes in the 144-cm^{-1} optical phonons. Such results infer a microwave thermal effect on the Ishihara ST-01 and N-ST01 specimens, whereas for the Degussa P-25 samples the microwaves also imparted a specific effect on the N-dopant states in contrast to the ST-01 systems where N dopant states seemed unaffected, at least as evidenced by the temperature–time profiles. Photodegradation of 4-chlorophenol under various conditions of UV–vis irradiation and conventional heating, as opposed to microwave heating, confirmed the specific microwave effect for the P-25 systems.

Acknowledgments

Financial support from the Japan Society for the Promotion of Science (JSPS) to S.H. through a Grant-in-aid for young scientists (No. B-21750210) is gratefully appreciated. One of us (NS) thanks Prof. Albini of the University of Pavia, Italy, for his kind hospitality through several semesters since 2002.

References

[1] V. Polshettiwar, R.S. Varma, Microwave-assisted organic synthesis and transformations using benign reaction media, Acc. Chem. Res. 41 (2008) 629–639.
[2] S. Horikoshi, H. Hidaka, N. Serpone, Environmental remediation by an integrated microwave/UV-illumination method. 1. Microwave-assisted degradation of rhodamine-b dye in aqueous TiO_2 dispersions, Environ. Sci. Technol. 36 (2002) 1357–1366.
[3] S. Horikoshi, N. Serpone, Photochemistry with microwaves. Catalysts and environmental applications, J. Photochem. Photobiol. C: Photochem. Rev. 10 (2009) 96–110.
[4] S. Horikoshi, M. Kajitani, H. Hidaka, N. Serpone, Investigation of factors that influence TiO_2 photoassisted degradations under simultaneous illumination by UV and microwave radiation fields, J. Photochem. Photobiol. A: Chem. 196 (2008) 159–164.
[5] H. Zhong, Y. Shaogui, J. Yongming, S. Cheng, Microwave photocatalytic degradation of rhodamine B using TiO_2 supported on activated carbon: mechanism implication, J. Environ. Sci. 21 (2009) 268–272.
[6] S. Yang, H. Fub, C. Sun, Z. Gao, Rapid photocatalytic destruction of pentachlorophenol in F–Si–co-modified TiO_2 suspensions under microwave irradiation, J. Hazard. Mater. 161 (2009) 1281–1287.
[7] X. Zhang, Y. Wang, G. Li, Effect of operating parameters on microwave assisted photocatalytic degradation of azo dye X-3B with grain TiO_2 catalyst, J. Mol. Catal. A: Chem. 237 (2005) 199–205.
[8] S. Horikoshi, M. Kajitani, N. Horikoshi, R. Dillert, D.W. Bahnemann, Use of microwave discharge electrodeless lamps (MDEL): II. Photodegradation of acetaldehyde over TiO_2 pellets, J. Photochem. Photobiol. A: Chem. 193 (2008) 284–287.
[9] S. Horikoshi, F. Sakai, M. Kajitani, M. Abe, A.V. Emeline, N. Serpone, Microwave-specific effects in various TiO_2 specimens. Dielectric properties and degradation of 4-chlorophenol, J. Phys. Chem. C 113 (2009) 5649–5657.
[10] S. Horikoshi, J. Tsuzuki, F. Sakai, M. Kajitani, N. Serpone, Microwave effect on the surface composition of the Urushibara Ni hydrogenation catalyst and improved reduction of acetophenone, Chem. Commun. (2008) 4501–4503.
[11] S. Horikoshi, F. Sakai, M. Kajitani, M. Abe, N. Serpone, Microwave frequency effects on the photoactivity of TiO_2: dielectric properties and the degradation of 4-chlorophenol, bisphenol A and methylene blue, Chem. Phys. Lett. 470 (2009) 304–307.
[12] S. Horikoshi, A. Matsubara, S. Takayama, M. Sato, F. Sakai, M. Kajitani, et al., Characterization of microwave effects on metal-oxide materials: zinc oxide and titanium dioxide, Appl. Catal. B: Environ. 91 (2009) 362–367.
[13] A.V. Emeline, V.N. Kuznetsov, V.K. Rybchuk, N. Serpone, Visible-light-active titania photocatalysts: the case of N-doped TiO_2s—properties and some fundamental issues, Int. J. Photoenergy (2008), doi:10.1155/2008/258394.
[14] N. Serpone, A.V. Emeline, V.N. Kuznetsov, V.K. Ryabchuk, Second generation visible-light-active photocatalysts: preparation, optical properties and consequences of dopants on the band gap energy of TiO_2, in: M. Anpo, P.V. Kamat (Eds.), Environmentally Benign Catalysts: The Development of Highly Active Photocatalysts for the Generation of Clean Energy and Their Applications to Environmental Problems (Nanostructure Science and Technology), Springer-Verlag Inc, New York, 2010, ISBN: 978-0-387-48441-9, (Chapter 3).
[15] J.A. Rengifo-Herrera, J. Kiwi, C. Pulgarin, N, S co-doped and N-doped Degussa P-25 powders with visible light response prepared by mechanical mixing of thiourea and urea. Reactivity towards *E. coli* inactivation and phenol oxidation, J. Photochem. Photobiol. A: Chem. 205 (2009) 109–115.
[16] Y. Nosaka, M. Matsushita, J. Nishino, A.Y. Nosaka, Nitrogen-doped titanium dioxide photocatalysts for visible response prepared by using organic compounds, Sci. Technol. Adv. Mater. 6 (2005) 143–148.
[17] H. Kisch, S. Sakthivel, M. Janczarek, D. Mitoraj, A low-band gap, nitrogen-modified titania visible-light photocatalyst, J. Phys. Chem. C 111 (2007) 11445–11449.
[18] T. Ohno, T. Mitsui, M. Matsumura, Photocatalytic activity of S-doped TiO_2 photocatalyst under visible light, Chem. Lett. 32 (2003) 364–365.
[19] K. Yanagisawa, Y. Yamamoto, Q. Feng, N. Yamasaki, Formation mechanism of fine anatase crystals from amorphous titania under hydrothermal conditions, J. Mater. Res. 13 (1998) 825–829.
[20] W. Kongsuebchart, P. Praserthdam, J. Panpranot, A. Sirisuk, P. Supphasrirongjaroen, C. Satayaprasert, Effect of crystallite size on the surface defect of nano-TiO_2 prepared via solvothermal synthesis, J. Crystal Growth 297 (2006) 234–238.
[21] M. Tanaka, H. Kono, K. Maruyama, Selective heating mechanism of magnetic metal oxides by a microwave magnetic field, Phys. Rev. B 79 (2009) 104420–104425.
[22] C. Di Valentin, G.-F. Pacchioni, A. Selloni, S. Livraghi, E. Giamello, Characterization of paramagnetic species in N-doped TiO_2 powders by EPR spectroscopy and DFT calculations, J. Phys. Chem. B 109 (2005) 11414–11419.
[23] V.N. Kuznetsov, N. Serpone, On the origin of the spectral bands in the visible absorption spectra of visible-light-active TiO_2 specimens, analysis and assignments, J. Phys. Chem. C 113 (2009) 15110–15123.
[24] M. Sato, M. Tanaka, Proceedings of the 12th AMPERE Conference, Karlsruhe, Germany, 2009.
[25] U. Balachandran, N.G. Eror, Raman spectra of titanium dioxide, J. Solid State Chem. 42 (1982) 276–282.
[26] B. Liu, L. Wen, X. Zhao, The structure and photocatalytic studies of N-doped TiO_2 films prepared by radio frequency reactive magnetron sputtering, Sol. Energy Mater. Sol. Cells 92 (2008) 1–10.
[27] A phonon is a quasi-particle characterized by the quantization of lattice vibrational modes in periodic, elastic crystalline solids having more than one atom type in the unit cell. Optical phonons are phonons that always have some minimum frequency of vibration, even when their wavelength is large, and are referred to as being optical because in ionic crystals such phonons are easily excited by infrared radiation creating a time-varying electrical dipole moment (infrared-active phonons). Raman-active optical phonons interact indirectly with light through Raman scattering. By contrast, acoustic phonons have fre-

quencies that become small at the long wavelengths and correspond to sound waves in the lattice.
[28] W.F. Zhang, Y.L. He, M.S. Zhang, Z. Yin, Q. Chen, Raman scattering study on anatase TiO_2 nanocrystals, J. Phys. D: Appl. Phys. 33 (2000) 912–916.
[29] S. Balaji, Y. Djaoued, J. Robichaud, Phonon confinement studies in nanocrystalline anatase-TiO_2 thin films by micro Raman spectroscopy, J. Raman Spectrosc. 37 (2006) 1416–1422.
[30] K.A. Akhilesh, M. Rajalakshmi, T.R. Ravindran, V. Sivasubramanian, Raman spectroscopy of optical phonon confinement in nanostructured materials, J. Raman Spectrosc. 38 (2007) 604–617.
[31] S.K. Gupta, R. Desai, P.K. Jha, S. Sahoo, D. Kirin, Titanium dioxide synthesized using titanium chloride: size effect study using Raman spectroscopy and photoluminescence, J. Raman Spectrosc. 41 (2010) 350–355.
[32] T. Kitagawa, A.T. Tu, Introduction to Raman spectroscopy, Kagaku-Dojin Publishing Co. Inc., Kyoto, Japan, 1988, ISBN: 4-7598-0172-3 (in Japanese).
[33] N.X. Xinh, A.A. Maradudin, R.A. Coldwell-Horsfall, Impurity induced first order Raman scattering of light by alkali–halide crystals, J. Phys. Fr. 26 (1965) 717–735.
[34] J. Shaw, D.K. Winslow, A. Karp, R.A. Wilson, Attenuation of hypersonic waves in sapphire and rutile at 2.8 Gc/sec and room temperature, Appl. Phys. Lett. 4 (1964) 28–30.
[35] T. Nomoto, A. Sasahara, H. Onishi, Optically excited near-surface phonons of TiO_2 observed by fourth-order coherent Raman spectroscopy, J. Chem. Phys. 131 (2009) (084703 (11 pages)).
[36] R.J.J. Riobóo, C. Serrano-Selva, M. Fernández-García, M.L. Cerrada, A. Kubacka, M. Fernández-García, A. de Andrés, Acoustic and optical phonons in EVOH–TiO_2 nanocomposite films: effect of aggregation, J. Lumin. 128 (2008) 851–854.
[37] S. Horikoshi, M. Kajitani, N. Serpone, The microwave-/photo-assisted degradation of bisphenol-A in aqueous TiO_2 dispersions revisited: re-assessment of the microwave non-thermal effect, J. Photochem. Photobiol. A: Chem. 188 (2007) 1–4.
[38] An interested reviewer noted that since we adopted the synthesis procedures reported in Refs. [15–18] the N-doped TiO_2 specimens would possess large amounts of urea residuals (impurities) on the particles' surfaces even if washed several times, and that therefore the photoreaction at 100 °C or higher would cause changes in the photoreaction rates and reaction selectivity, among others. In the present case, we followed very closely the synthesis procedures reported in the cited references, and have calcined the resulting N-doped TiO_2 specimens in a manner very similar to those reported as indicated in the experimental section. Nonetheless the reviewer does raise a very good point of potential carbonaceous residues remaining from syntheses of doped TiO_2 when using organic compounds as a source of dopant constituents. After calcining the N-doped products at 400 °C for 1 h, or higher (e.g. 500 °C for 5 hours), it is unlikely that urea was left as an impurity. More important is the likelihood that C may also be a dopant in the TiO_2 network under such experimental conditions, which would certainly cause some changes in the "selectivity" and "photoreaction dynamics". However, the UV–vis diffuse reflectance spectra showed no evidence for C doping and none was reported in Refs. [15–18] either. In fact, the UV–vis spectra of our N-doped samples are similar to those of many other such spectra reported for N-doped TiO_2s and very dissimilar with spectra reported for C-doped and/or C,N-codoped TiO_2s (see for example the extensive literature cited in Refs. [13,14]).
[39] A. Orlov, M.S. Tikhov, R.M. Lambert, Application of surface science techniques in the study of environmental photocatalysis: nitrogen-doped TiO_2, C.R. Chim. 9 (2006) 794–799.
[40] J. Chen, L.-B. Lin, F.-Q. Jing, Theoretical study of F-type color center in rutile TiO_2, J. Phys. Chem. Solids 62 (2001) 1257–1262.
[41] A.V. Emeline, N.V. Sheremetyeva, N.V. Khomchenko, V.K. Ryabchuk, N. Serpone, Photoinduced formation of defects and nitrogen stabilization of color centers in N-doped titanium dioxide, J. Phys. Chem. C 111 (2007) 11456–11462.
[42] T. Tachikawa, M. Fujitsuka, T. Majima, Mechanistic insight into the TiO_2 photocatalytic reactions: design of new photocatalysts, J. Phys. Chem. C 111 (2007) 5259–5275.
[43] S. Sakthivel, H. Kisch, Photocatalytic and photoelectrochemical properties of nitrogen-doped titanium dioxide, ChemPhysChem 4 (2003) 487–490.
[44] Z. Cheng, Y. Li, What is responsible for the initiating chemistry of iron-mediated lipid peroxidation: an update, Chem. Rev. 107 (2007) 748–766.
[45] J.A. Rengifo-Herrera, K. Pierzchala, A. Sienkiewicz, L. Forró, J. Kiwi, C. Pulgarin, Abatement of organics and *E. coli* by N,S co-doped under UV and UV–vis light. Implications of the formation of singlet oxygen ($^1O_2$) under visible light, Appl. Catal. B 88 (2009) 398–406.
[46] T. Daimon, T. Hirakawa, M. Kitazawa, J. Suetake, Y. Nosaka, Formation of singlet molecular oxygen associated with the formation of superoxide radicals in aqueous suspensions of TiO_2 photocatalysts, Appl. Catal. A 340 (2008) 169–175.
[47] D. Sawyer, J.S. Valentine, How super is superoxide? Acc. Chem. Res. 14 (1981) 393–400.